RIM1 confers sustained activity and neurotransmitter vesicle anchoring to presynaptic Ca2+ channels

Kiyonaka Shigeki [1], Wakamori Minoru [1], Miki Takafumi [1], Uriu Yoshitsugu [1], Nonaka Mio [2], Bito Haruhiko [2], Beedle Aaron M. [3 4], Mori Emiko [1], Hara Yuji [1 3 4], De Waard Michel [5], Kanagawa Motoi [3 4], Itakura Makoto [6], Takahashi Masami [6], Campbell Kevin P. [3 4], Mori Yasuo [1 *]

[1] *Department of Synthetic Chemistry and Biological Chemistry Kyoto University, Graduate School of Engineering, Kyoto University, Katsura Campus, Nishikyo-ku, Kyoto 615-8510,JP*

[2] *Department of Neurochemistry University of Tokyo, University of Tokyo Graduate School of Medicine, Hongo 7-3-1, Bunkyo-ku, Tokyo 113-0033,JP*

[3] *Departments of Physiology and Biophysics, Internal Medicine, and Neurology University of Iowa, University of Iowa Roy J. and Lucille A. Carver College of Medicine, 285 Newton Road, Iowa City, Iowa 52242-1101,US*

[4] *HHMI, Howard Hughes Medical Institute Howard Hugues Institute , Howard Hughes Medical Institute,US*

[5] *Canaux calciques , fonctions et pathologies INSERM : U607, CEA : DSV/IRTSV, Université Joseph Fourier - Grenoble I, 17, rue des martyrs 38054 Grenoble,FR*

[6] *Department of Biochemistry Kitasato University School of Medicine, Kitasato University School of Medicine, Kitasato 1-15-1, Sagamihara, Kanagawa 228-8555,JP*

* Correspondence should be adressed to: Yasuo Mori <mori@sbchem.kyoto-u.ac.jp>

Abstract

The molecular organization of presynaptic active zones (AZs) is central to neurotransmitter release triggered by depolarization-induced Ca^{2+} influx. Here, we demonstrate a novel interaction between AZ components, RIM1 and voltage-dependent Ca^{2+} channels (VDCCs), that controls neurotransmitter release. RIM1 associates with VDCC β-subunits via its C-terminus to markedly suppress voltage-dependent inactivation among different neuronal VDCCs. Consistently, in neuroendocrine PC12 cells, acetylcholine release is significantly potentiated by the full-length and C-terminal RIM1 constructs, but membrane docking of vesicles is enhanced only by the full-length RIM1. The dominant negative β construct BADN, that disrupts the RIM1-β association, accelerates inactivation of native VDCC currents, and suppresses vesicle docking and acetylcholine release in PC12 cells, and inhibits glutamate release in cultured cerebellar neurons. Thus, RIM1 association with β in the AZ supports release via two distinct mechanisms: sustaining Ca^{2+} influx through inhibition of channel inactivation; and anchoring of neurotransmitter-containing vesicles in the vicinity of VDCCs.

MESH Keywords Animals ; Animals, Newborn ; Brain ; cytology ; metabolism ; Calcium ; metabolism ; Cells, Cultured ; GTP-Binding Proteins ; physiology ; Gene Expression Regulation ; Humans ; Mice ; Models, Molecular ; Nerve Tissue Proteins ; physiology ; Neurons ; cytology ; Neurotransmitter Agents ; metabolism ; Presynaptic Terminals ; physiology ; Protein Subunits ; metabolism ; Qa-SNARE Proteins ; metabolism ; Rats ; Rats, Wistar ; Synaptic Transmission ; Synaptic Vesicles ; physiology ; Transfection ; methods ; Two-Hybrid System Techniques ; Voltage-Dependent Anion Channels ; physiology

Introduction

The presynaptic active zone (AZ) is the specific site for impulse-evoked exocytosis of neurotransmitters at synapses of the nervous system across species1,2. Fine regulation of AZ neurotransmitter release is integral to nervous system adaptive functions including learning, memory, and cognition. The molecular organization of AZs, where synaptic vesicles are docked in close vicinity to VDCCs at the presynaptic membrane, is essential for the control of neurotransmitter release triggered by depolarization-induced Ca^{2+} influx. The spacing between VDCCs and vesicles influences the dynamic properties of synaptic transmission3. However, molecular determinants that maintain vesicles and VDCCs within a physiologically appropriate distance have remained elusive.

RIM1, originally identified as a putative effector for the synaptic vesicle protein Rab3 (ref. 4), is part of the RIM superfamily whose members share a common C_2B domain at their C-termini5. RIM1 interacts with other AZ protein components, including Munc13, ELKS/CAST, RIM-BP, or Liprins, to form a protein scaffold in the presynaptic nerve terminal6–10. Mouse knockouts revealed that, in different types of synapses, RIM1 is essential for different forms of synaptic plasticity9,11. In the CA1-region Schaffer-collateral excitatory synapses and in GABAergic synapses, RIM1 maintains normal neurotransmitter release and short-term synaptic plasticity. In excitatory CA3-region mossy fibre synapses and cerebellar parallel fibre synapses, RIM1 is necessary for presynaptic long-term synaptic plasticity. In autapses, the RIM1 deletion significantly reduces the readily releasable pool of vesicles, alters short-term plasticity and the properties of evoked asynchronous release12. However, in spite of the progress in understanding RIM1 functions, the mechanisms by which RIM1 acts remain unknown. Moreover, the physiological roles played by other RIM isoforms (RIM2, RIM3, and RIM4)5 remain unclear.

Multiple types of VDCCs distinguished on the basis of biophysical and pharmacological properties coexist in neurons13. High voltage-activated types of VDCCs essential for neurotransmitter release include N-, P/Q-, R-, and L-types14–16. VDCCs are heteromultimeric protein complexes comprised of the pore-forming α_1, designated as Ca_v, and auxiliary subunits α_2/δ, β, and γ17. The α_1 -subunit is encoded by 10 distinct genes, whose correspondence with functional types is largely elucidated13,17. VDCC complexes are associated with presynaptic and postsynaptic proteins including syntaxin, SNAP-25, synaptotagmin, CASK, and Mint primarily via interactions with the α_1-subunit18–25. The β-subunit interacts with the α_1-subunit to enhance functional channel trafficking to the plasma membrane26,27 and to modify multiple kinetic properties28; it also interacts with other proteins29–31. Therefore, it is intriguing to investigate whether β-subunits are involved in targeting VDCC complexes to specific subcellular machinery at AZs for neurotransmitter release through yet unidentified interactions. Here, we demonstrate a novel molecular interaction between RIM1 and VDCC β-subunits, both of which are essential AZ proteins. The RIM1-β interaction supports the function of RIM1 in neurotransmitter release via two distinct mechanisms: the anchoring of neurotransmitter-containing vesicles in the vicinity of VDCCs; and sustaining Ca^{2+} influx through the inhibition of voltage-dependent inactivation.

Results

VDCC β-subunits directly interact with RIM1

To identify β-subunit interacting proteins that regulate AZ organization, we performed yeast two-hybrid screening with a mouse brain complementary DNA library using the full length rat β_{4b}-subunit as a bait. The β_4-subunit was chosen because spontaneous β_4-mutant mice lethargic32 have clear neurological defects suggesting that β_4-containing VDCCs are physiologically significant in the brain. Screening identified a clone (#2-5) encoding the C-terminal region (1079–1463) of the mouse RIM1 protein4 including the C_2B domain (Fig. 1a). Subsequent two-hybrid assays using β_{4b} mutants revealed that residues 49-410 containing major structural motifs such as Src homology 3 (SH3) domain, α_1-interacting domain known as BID, and guanylate kinase (GK) domain, are required for the interaction of β_{4b} with the RIM1 C-terminus (Fig. 1b). β_{2a} also showed RIM1 interaction. in vitro pulldown assays using GST fusion constructs identified the RIM1 C-terminus (1079–1463) as a major β_4-interaction domain likely formed in concert by two adjacent subdomains (1079–1257 and 1258–1463; Fig. 1c and Supplementary Fig. 1). An in vitro binding assay using purified β_4 and RIM1 recombinants revealed a dissociation constant (K_d) of 35.1 nM for RIM1(1079–1463) significantly lower than 481 nM for RIM1(1079–1257) and 717 nM for RIM1(1258–1463) (Fig. 1d and Supplementary Fig. 2). These results, as well as the successful coimmunoprecipitation of full-length RIM1 with β_{4b} (Fig. 1e), suggest a direct protein-protein interaction between RIM1 and β_4.

RIM1 physically associates with native VDCCs in the brain

Association between native VDCCs and RIM1 was characterized biochemically using VDCC complexes enriched from mouse brains through microsome preparation, KCl wash, solubilization, heparin purification, and sucrose density gradient fractionation25. Western blot analysis of sucrose gradient fractions showed cosedimentation of RIM1 with $Ca_v2.1$ and β_4 (Fig. 2a). Statistical analysis of cosedimentation data reveals complete overlap of $Ca_v2.1$ and β_4, confirming their association in the VDCC complex (Fig. 2b). RIM1 sedimented in overlapping minor and major peaks: the latter completely overlapped with VDCC subunits, whereas the former did not cosediment with VDCC and likely represents a subset of RIM1 in a smaller, non-VDCC complex. Syntaxin, a VDCC interacting protein18–21, showed similar cosedimentation with RIM1. Immunoprecipitation analysis of heparin purified samples confirmed that the cosedimentation of RIM1 is due to its specific interaction with VDCC subunits (Fig. 2c). Anti-β_4 antibody precipitated RIM1 from wild-type mice but not from lethargic mice that express truncated β_4 protein lacking the α_1-interacting region32,33. It is unlikely that the β_4 isoform exclusively mediates the RIM1-VDCC association in the brain, since wild-type and lethargic mice were indistinguishable in the sucrose gradient profile (Fig. 2d). A β_{4b} fusion construct was designed as a dominant negative (beta-AID dominant negative (BADN)) suppressor to dissociate the activity of β-binding proteins such as RIM1 from the functional VDCC complex (Supplementary Fig. 3a–c). As residues 49-410 of the entire 519 amino acid β_{4b} sequence are required for RIM1 binding (Fig. 1b), BADN was based upon the " full-length" β_{4b} in order to efficiently quench RIM1. BADN also carries the β-interacting AID region from $Ca_v2.1$ buried at the α_1-binding site33. Since the intermolecular association of BADN with VDCC α_1 is inhibited by the intramolecular occlusion of the α_1-binding site in BADN, BADN overexpression should deprive native β-subunits of RIM1 without affecting their association with α_1. in vitro binding and coimmunoprecipitation experiments showed the ability of BADN to bind to RIM1 but not to the AID-containing I–II linker region of Ca_v 2.1 (Supplementary Fig. 3d,e). Importantly, the native RIM1-β association in partially purified brain VDCCs was disrupted by 8 hr coincubation with 100 nM GST fusion proteins for BADN or RIM1(1079–1463) (Fig. 2e). in vitro binding of β_4 to RIM1(1079–1463) rapidly decayed with the addition of excess BADN (200 nM), indicating that this disruption is attributable to displacement of binding partners in the native association (Supplementary Fig. 3f). These results provide evidence for a physiological association between native RIM1 and P/Q-type VDCCs via the β-subunit in brain.

RIM1 targets to VDCC via β-subunits at the plasma membrane

In recombinant HEK293 cells, β_{4b} and RIM1 were concentrated at the plasma membrane by coexpression of the P/Q-type $Ca_v2.1$ α_1-subunit, whereas they were diffusively colocalized throughout the intracellular area in the absence of $Ca_v2.1$ (Fig. 3a and Supplementary Fig. 4a,b): F_{PM}/F_{CYT} (ratio of the fluorescent intensity at the plasma membrane (PM) to that in the cytoplasm (CYT)) was 0.52 ± 0.07 and 0.48 ± 0.07 with $Ca_v2.1$ and 0.10 ± 0.02 and 0.08 ± 0.02 without $Ca_v2.1$ for β_{4b} and RIM1, respectively. RIM1 localization to the plasma membrane via a membrane-targeted β-binding domain27 comprised of CD8 and the $Ca_v2.1$ I–II linker was elicited only after β_{4b} coexpression (Fig. 3b and Supplementary Fig. 4c,d): F_{PM}/F_{CYT} was 0.29 ± 0.03 and 0.27 ± 0.02 with β_{4b} and 0.08 ± 0.01 and 0.08 ± 0.02 without β_{4b} for the $Ca_v2.1$ I–II linker and RIM1, respectively. Notably, the $Ca_v2.1$-mediated plasma membrane colocalization of RIM1 and β_{4b} or the β_{4b}-mediated colocalization of RIM1 and the $Ca_v2.1$ I–II linker was disrupted by BADN. In the presence of BADN, F_{PM}/F_{CYT} was 0.56 ± 0.11 and 0.19 ± 0.04 for β_{4b} and RIM1, respectively; and F_{PM}/F_{CYT} was 0.33 ± 0.04 and 0.13 ± 0.04 for the $Ca_v2.1$ I–II linker and RIM1, respectively. Thus, the RIM1-β_{4b} interaction is likely to be essential for assembly of RIM1 with VDCC at the plasma membrane. In cultured hippocampal neurons, RIM1 and β_{4b} both accumulated near presynaptic termini, in parallel with $Ca_v2.1$ clustering. These events had a substantially later onset than synaptogenesis shown by synapsin I clustering observed at 8 days in vitro (DIV) (Fig. 3c,d). Quantitative imaging demonstrated that overexpression of either BADN or the RIM1 C-terminus (RIM1(1079–1463)) impaired the $Ca_v2.1$ clustering in presynaptic varicosities (Fig. 3e,f). The coincident targeting of RIM1 and β_{4b}, as well as the blockade of $Ca_v2.1$ accumulation by quenching of RIM1 and βs, suggests that the RIM1-β interaction regulates localization of VDCCs at the presynaptic membrane. As RIM1 interacts with multiple proteins (Fig. 1a), the RIM1 effect observed using BADN and RIM1(1079–1463) could also be attributed to the quenching of other RIM interactions at different subcellular locations. However, a recent immunostaining study showed that the staining intensities for $Ca_v2.2$ and RIM co-vary at a giant calyx-type synapse34, consistent with the idea that they are both components of transmitter release sites.

RIM1-β interaction modulates inactivation of VDCCs

To elucidate the functional significance of direct RIM1-β_4 coupling, we characterized whole-cell Ba^{2+} currents through recombinant VDCCs expressed as $\alpha_1\alpha_2/\delta\beta$ complexes containing various neuronal α_1-subunits, N-type $Ca_v2.2$, P/Q-type $Ca_v2.1$, R-type $Ca_v2.3$, and L-type $Ca_v1.2$ in BHK cells. The most prominent RIM1 effect on VDCC currents was observed on inactivation parameters. Inactivation was dramatically decelerated in N-, P/Q-, R-, and L-type currents (Fig. 4a,b). The same set of VDCC types also showed a significant depolarizing shift in the voltage dependence of inactivation (Fig. 4c,d). In P/Q-type (with β_{4b}), RIM1 shifted the half inactivation potential ($V_{0.5}$) by +24.6 mV eliciting an inactivation curve with a component susceptible to inactivation induced at high voltages ($V_{0.5}$ (vector) = −45.9 mV, $V_{0.5}$ (RIM1) = −21.3 mV) and a non-inactivating component (Supplementary Table 1). In N- and R-types, RIM1 provoked a switch in the major phase of biphasic inactivation curves from low voltage-induced ($V_{0.5}$ and ratio; −64.5 mV and 0.91 for N, and −78.2 mV and 0.91 for R) to high voltage-induced ($V_{0.5}$ and ratio; −20.8 mV and 0.61 for N, and −27.9 mV and 0.53 for R). The L-type inactivation curve remained monophasic, however the non-inactivating component was significantly augmented by RIM1 (from 0.07 to 0.25). In P/Q-type, similar RIM1 effects on inactivation were observed with all other β-subunits tested (Fig. 4a,c and Supplementary Table 2). Furthermore, the C-terminal truncated mutants RIM1(1079–1463) and RIM1(1258–1463), but not RIM1(1079–1257), successfully slowed P/Q-type (with β_{1a}) current inactivation (Fig. 4a,c and Supplementary Table 3). After RIM1 coexpression, single-channel P/Q-type currents clearly demonstrated prolongation of mean time between first channel opening and last closing within a trace during 750-ms depolarizations to +20 mV without significant changes in amplitude (0.59 pA) (Fig. 4e). This observation corresponds well with the whole-cell data and suggests that RIM1 predominantly stabilizes the non-inactivating mode35. Currents evoked by trains of action potential (AP) waveforms, a more physiological voltage-clamp protocol used to reveal closed-state inactivation36, further support the profound suppression of voltage-dependent inactivation by RIM1 (Fig. 4f). The observed effect of RIM1 on VDCC inactivation is attributable to its association with the β-subunit, since replacement of β_4 with a C-terminal truncation construct β_4-GK37, that directly interacts with α_1 but lacks the ability to bind RIM1 (Supplementary Fig. 5a,b), failed to significantly affect inactivation of N-type current (Supplementary Fig. 5c,d and Supplementary Table 4). In addition, BADN significantly diminished the RIM1 effect on P/Q channel inactivation (Supplementary Fig. 5e,f and Supplementary Table 5). When 5 mM Ca^{2+} was used as a physiological charge carrier capable of inducing both Ca^{2+}-dependent and voltage-dependent inactivation38, RIM1 still exerted prominent suppressive effects on inactivation in P/Q-type currents expressed in HEK293 cells (Fig 5a,b and Supplementary Table 6). Importantly, in rat pheochromocytoma PC12 neuroendocrine cells, BADN or co-application of siRNAs specific for suppression of RIM1 and RIM2 expression (Supplementary Fig. 7a) accelerated inactivation and shifted the inactivation curve toward the hyperpolarizing direction (Fig. 5c,d and Supplementary Table 7). This supports a physiologically significant role for RIM-mediated VDCC modulation via the β-subunit. Notably, as observed in RIM1-expressing cells, voltage-dependent inactivation of presynaptic VDCC currents at membrane potentials ≥ −40 mV was previously demonstrated39. Thus, RIM1 exerts strong suppressive effects on the kinetics and voltage dependence of inactivation of VDCC currents.

RIM1 effects on other functional current parameters such as voltage dependence of activation, activation kinetics, and current densities at different voltages in current-voltage relationships, distinguish VDCCs into two different groups (Fig. 6 and Supplementary Table 1). In β_{4b}-expressing BHK cells, the current densities of N-and P/Q-types were significantly augmented by RIM1, while those of R- and L-types

were unaffected by RIM1 (Fig. 6c,d). In P/Q-type, RIM1(1079–1463), that binds β, was sufficient to enhance current density (Fig. 6c). By contrast, activation speeds were significantly decelerated and activation curves were shifted toward positive potentials by RIM1 in R- and L-types, but not in N- and P/Q-types (Fig. 6a,b). Replacement of β_{4b} with other β isoforms abolished the augmentation of P/Q-type current densities by RIM1 (Supplementary Fig. 6a), but slowed activation speed of P/Q-type by RIM1 (Fig. 6b). The RIM1 positive shift in activation curve was also elicited by β_{2a} in P/Q-type (Supplementary Fig. 6b). Thus, N- and P/Q-type currents responded differently than R- and L-type currents to RIM1 in terms of activation parameters and current densities, perhaps reflecting different subcellular localizations or functions of these channel subsets.

RIM1-β binding anchors neurotransmitter vesicles to VDCC

We directly observed vesicles docked to the plasma membrane using evanescent wave microscopy, which illuminates only the subcellular area from the surface to a depth of less than 100 nm by total internal reflection fluorescence (TIRF). Dense-core vesicles were identified by a fusion protein of neuropeptide Y (NPY) and the fluorescent protein Venus in PC12 cells. The overlapping distribution of NPY-Venus, VAMP-DsRedmonomer, and RIM1-DsRedmonomer indicates that transmitter-filled synaptic vesicles are identified using fluorescent signals of NPY-Venus (Fig. 7a). The co-distribution is likely specific for RIM1, since caveolin-1-EGFP failed to colocalize with VAMP-DsRedmonomer. As demonstrated in Fig. 7b and 7c, the number of docked vesicles was increased significantly by expression of the full-length RIM1, whereas it was unaffected by RIM1(11–399), that forms a ternary complex with Rab3 and Munc13 via Zn^{2+} finger critical for neurotransmitter release40, or by RIM1(400–1078). Importantly, BADN as well as RIM1(1079–1463) significantly attenuated the number of docked vesicles. These inhibitory effects of BADN and RIM1(1079–1463) on vesicle docking are most likely to be exerted by quenching endogenous full-length RIMs, or by saturating RIM1 interaction sites on VDCC β subunits, respectively. The BADN effect is not due to a reduction in the densities of VDCCs in PC12 cells, as BADN failed to significantly affect current densities (Fig. 5c). Thus, the 'full-length' structure is likely to be essential for RIM1 to anchor neurotransmitter vesicles to VDCCs.

RIM1-β interaction enhances neurotransimitter release

The physiological relevance of RIM1 interactions with the VDCC complex was studied by assessing neurotransmitter release from PC12 cells in which diverse high voltage-activated VDCC types have been precisely characterized35,41 (Supplementary Fig. 7c,d). PC12 cells were transfected with RIM1 construct cDNAs along with the choline acetyltransferase (ChAT) gene that synthesizes ACh for synaptic vesicles42. ACh release, triggered by Ca^{2+} influx in response to high-K^+ (elevation of extracellular K^+ concentration from 5.9 mM to 51.1 mM) membrane depolarization, was significantly potentiated by full-length RIM1 (Fig. 8a and Supplementary Fig. 7e). ACh release was also enhanced by the Rab3-interacting N-terminal RIM1(11–399) and by the C-terminal RIM1(1079–1463) that maintains VDCC currents, but not by the middle RIM1(400–1078). In contrast, BADN significantly suppressed ACh release. In cultured cerebellar neurons, similar suppression by BADN and potentiation by the full-length RIM1 were observed for high-K^+-induced glutamate release (Fig. 8b). The results suggest that RIM1 potentiates neurotransmitter release through its interaction with VDCC β in neuronal and neuron-like cells.

Discussion

The present investigation reveals a novel physical association between the presynaptic AZ proteins RIM1 and VDCC β-subunits. The results of yeast two-hybrid assay, in vitro binding assay, and coimmunoprecipitation experiments have identified a RIM1-VDCC complex formed by direct interaction of the β-subunit with the α_1-subunit AID region and the RIM C-terminus 1079–1463 (Fig. 1). The identification of native RIM1-VDCC complexes in brain (Fig. 2), the colocalization of RIM1 with VDCC subunits at the plasma membrane and the presynapse, and the disruption of such localization and complex formation by BADN (Fig. 3) support a physiological role for the RIM1-β association. Further biochemical and functional analyses (Fig. 1 and Fig. 4) suggest that RIM1(1079–1257) and RIM1(1258–1463) are the primary β-subunit binding site and modulatory region, respectively, in the RIM1 protein. While our experiments showed the RIM1-β_4 interaction, RIM1 of wild-type and lethargic brains was indistinguishable by sucrose gradient profile (Fig. 2a,d). It has been previously reported that immunolocalization of $Ca_v2.1$ and $Ca_v2.2$ in the brain and properties of P-type currents in Purkinje neurons are indistinguishable between wild-type and lethargic mice32. This has been attributed to the rescue of β_4 deficiency by remaining β_1, β_2, and β_3. We expect a similar compensatory mechanism may also occur in the RIM1-β interaction in lethargic mice. Therefore, the β_4 isoform is unlikely to exclusively mediate the RIM1-VDCC association in the brain.

The RIM1-β association enables RIM1 to play a dual physiological role in neurotransmitter release: sustaining Ca^{2+} influx through the functional regulation of VDCCs and anchoring vesicles to VDCCs (Supplementary Fig. 8). Among the functional parameters of VDCCs, those which are related to voltage-dependent inactivation are most prominently modified by RIM1 through the β interaction (Fig. 4). Inactivation kinetics are markedly decelerated resulting in the predominance of high voltage inactivation and an inactivation-resistant current component in the 2-s prepulse protocol. Similarly modulated inactivation properties of P/Q-type VDCC by RIM2α, RIM3γ, or RIM4γ (unpublished results), which all carry the C_2B domain, suggest that this function is a common feature for the RIM family5. Suppression by BADN of the RIM1-mediated inactivation in both the recombinant (Supplementary Fig. 5e,f) and native VDCCs (Fig. 5c)

provides evidence that RIM1 exerts observed effects through the RIM1-β association. This is supported by our finding that β_4-GK, which binds to α_1 (ref. 37) but not to RIM1, failed to mediate RIM1 effects on N-type channels (Supplementary Fig. 5a–d). Although detailed molecular mechanisms underlying inactivation are yet to be elucidated, previous mapping of the molecular determinants for voltage-dependent inactivation kinetics43 may suggest that RIM1-β complexes bound to the I–II linker AID further act on adjacent segment S6 of repeat I to hinder its conformational transition to the inactivated state. Alternatively, RIM1 may immobilize the β-subunit and the process of inactivation by slowing the movement of the I–II loop44,45. When voltage-dependent inactivation is thus suppressed, responses of Ca^{2+} sensors such as synaptotagmins to Ca^{2+} influx may be potentiated at depolarizing membrane potentials that induce voltage-dependent inactivation when RIM1 is absent. Since RIM1 virtually abolished VDCC inactivation elicited by a train of AP waveforms (Fig. 4f), certain forms of synaptic depression via closed-state inactivation36 may be minimized by RIM1 at AZs. The impact of the RIM1-β association to delay VDCC inactivation may explain recent findings using the RIM1α knockout mouse demonstrating that RIM1 is important for the late stage asynchronous neurotransmitter release whereas synaptotagmin I is involved in the earlier synchronous release12. With P/Q- and N-type channels, the RIM1-β association significantly affected channel activity as well: current densities were nearly doubled by RIM (Fig. 6c). Thus, RIM1 can maintain and enhance depolarization-induced Ca^{2+} influx to support neurotransmitter release at presynaptic AZs.

Regarding the role of RIM1 in vesicle anchoring to VDCC at the plasma membrane, 'full-length' RIM1 is required to mediate vesicle anchoring, in contrast to the RIM1 suppression of VDCC inactivation which only requires the RIM1 C-terminus. Taking into consideration the direct RIM1-Rab3 association and the regulation of tethering and/or priming of synaptic vesicles by Rab3 (ref. 40), it is likely that simultaneous interactions of RIM1 with vesicle-associated Rab3/Munc13 via the N-terminal Zn^{2+}-finger domain and with the VDCC β -subunit via the C-terminal C_2B domain underlie, at least in part, the maintenance of a close proximity between VDCCs and vesicles, thereby regulating the dynamic properties of synaptic transmission3. Supporting this idea, BADN and RIM1(1079–1463) significantly suppressed vesicle docking in PC12 cells (Fig. 7c). In our experiments, however, RIM1 and β-subunit co-targeting to the presynaptic site was observed only after early synapse formation (Fig. 3). It is important to note that the interaction of Mint and CASK with VDCC α_1 -subunits via their C-termini22,23 may also direct channel targeting in parallel of, or prior to, RIM1-β-subunit complex formation. Notably, our observation is consistent with a previous report46 stating that the loss of UNC10/RIM caused a reduction in membrane-contacting synaptic vesicles within 30 nm of the dense projection at Caenorhabditis elegans neuromuscular junctions. Furthermore, in RIM1α-defecient mice, the decay of excitatory postsynaptic currents (EPSCs) during 14 Hz trains of presynaptic stimulation is abolished, while the rate at which the readily releasable vesicle pool is refilled is indistinguishable between the wild-type and RIM1α mutant mice12. These data suggest that RIM1-mediated vesicle anchoring to VDCCs may enable a rapid depletion of vesicle pools such that available vesicles are exhausted leading to EPSC decay. In this scenario, RIM1 knockout would minimize rapid vesicle release enabling the readily releasable pool to be maintained and thus prevent EPSC decay. More recently, Schoch et al. have reported mice deficient in both RIM1α and RIM2α show lethality due to defects in Ca^{2+}-triggered release despite normal AZ length and normal spontaneous neurotransmitter release47. Combined, these studies support our model (Supplementary Fig. 8), predicting a dual function for the RIM1-β interaction in neurotransmitter release by coordinating the molecular constituents and Ca^{2+} signaling in AZs.

Previous reports have demonstrated the functional impact of syntaxin, synaptosome-associated protein (SNAP-25), and synaptotagmin on VDCCs through physical association with the 'synprint' region in the II–III linker of α_1-proteins19–21. Physical association of RIM directly via the C_2A domain with the synprint10 and indirectly via the RIM-binding protein (RIM-BP) with the α_1 C-terminal tail have been also reported48 (Fig. 1a). However, RIM1 regulation of VDCCs may be independent of the synprint- or RIM-BP-mediated association, because RIM1(1079–1463), which lacks both the C_2A domain necessary for synprint binding10 and the PXXP motif for the RIM-BP binding is still sufficient to inhibit VDCC inactivation (Fig. 4a,c). This is supported by our observation that BADN (Supplementary Fig. 5e,f) or replacement of β with β_4-GK (Supplementary Fig. 5a–d), is sufficient to disrupt RIM1 effects on inactivation. Syntaxin and SNAP-25 have been proposed to inhibit VDCC-mediated Ca^{2+} influx via a hyperpolarizing shift of the inactivation curve in the absence of vesicle docking at VDCC sites19,21, while our finding by contrast implies enhancement or maintenance of the Ca^{2+} influx via interaction with RIM1 during the docking of vesicles. Importantly, previous reports suggest that RIM1 is involved in the modification of the release apparatus at a late stage in the vesicle cycle9, particularly in the post-docking step49. In early phases of vesicle docking, interactions of VDCC α_1 with syntaxin/SNAP2519–21 and Mint/CASK22,23 may play primary roles, eliciting partial resistance to BADN suppression of vesicle docking (Fig. 7c). Thus, the α_1 protein associations and the RIM1-β association may be distinct interactions that contribute at different stages of vesicle cycling to control the Ca^{2+} supply from the source, namely the VDCC, in addition to regulating the proximity between the Ca^{2+} source VDCC and the target Ca^{2+} sensors at the presynaptic AZ.

Methods

cDNA expression, cell culture, molecular modeling, recombinant proteins, infection with Sindbis viruses

Methods for cDNA cloning and expression, cell culture, molecular modeling of BADN, preparation of GST fusion proteins and purified β_{4b}-subunit recombinants, and preparation and infection of Sindbis viruses can be found in Supplementary Methods.

Yeast two-hybrid screening and β-galactosidase assay

Rat β_{4b}-subunit (GenBank accession number XM_215742) subcloned into pGBK-T7 was used as a bait to screen a mouse brain pACT2 library in the yeast strain AH109 (Clontech). 1.5×10^6 transformants plated to synthetic medium lacking adenine, histidine, leucine, and tryptophan. His^+ colonies were assayed for β-galactosidase activity by a filter assay. Of the transformants, 103 were His^+, of which 21 were also $LacZ^+$. Prey clone #2-5 encoding RIM1(1079–1463) (NM_053270) was isolated.

in vitro binding of the purified proteins, GST-pulldown and coimmunoprecipitation experiments

RIM1-GST fusion proteins at various concentrations were incubated with 50 pM purified recombinant β_4-subunits for 3 h at 4 °C. Proteins were subjected to western blotting (WB) with the anti-β_4 antibody raised against the peptide ENYHNERARKSRNRLS. The densities of protein signals, obtained using NIH image under the linear relationship with the applied amount of proteins (Supplementary Fig. 2a), were normalized to the densities from the maximal binding. For pulldown assay, the cell lysate was incubated with glutathione-Sepharose beads bound with purified fusion proteins. The proteins were characterized by WB with anti-myc antibody (invitrogen). For coimmunoprecipitation, the cell lysate was incubated with anti-FLAG M2 monoclonal antibody (Sigma), and the immunocomplexes were characterized by WB with anti-myc antibody. For details, see Supplementary Methods.

Biochemistry of native neuronal VDCC complexes

VDCC complexes were partially purified from brains of C57BL6 mice or lethargic mice (B6EiC3Sn-a/A-Cacnb4 ^{lh}/J, Jackson Laboratory) as previously reported25. KCl washed microsomes (50 mg) were solubilized in Buffer I (for buffers, see Supplementary Table 8), and centrifuged at 142,000 × g for 37 min. The supernatant was incubated with Heparin-agarose (Sigma); agarose was washed with Buffer II and III prior to elution with Buffer IV. After elution, samples were diluted to 150 mM NaCl by addition of Buffer V, and concentrated using centrifugal filter devices (Millipore). The samples were applied to 5–40 % sucrose density gradients (Buffer VI) and were centrifuged at 215,000 × g for 90 min. WB was performed using antibodies against RIM (BD biosciences), $Ca_v2.1$ (Alamone), syntaxin (Sigma), and β_4 (described above). Western blot band densities (NIH image) were normalized from 4 to 5 independent experiments.

For immunoprecipitation, partially purified neuronal VDCC complexes were incubated with protein A-agarose coupled to anti-β_4 or anti-RIM1 antibodies4. Immunoprecipitated proteins were subject to WB with antibodies against RIM or $Ca_v2.1$. To disrupt the physiological association of native RIM1 with VDCC β_4, partially purified VDCC complexes were incubated with 200 nM GST-BADN and GST-RIM1(1079–1463) for 8h at 4 °C prior to immunoprecipitation.

Confocal imaging

32 h after transfection, HEK293 cells or PC12 cells were plated onto poly-L-lysine coated glass coverslips. 56 h after transfection, Hoechst 33342 (1 μg/ml, Dojindo) was added to stain nuclei. The imaging was performed in modified Ringer's buffer that contained (in mM): 130 NaCl, 3 KCl, 5 $CaCl_2$, 1.5 $MgCl_2$, 10 glucose, 10 HEPES (pH 7.4). Fluorescence images were acquired with a confocal laser-scanning microscope (Olympus FV500). For details, see Supplementary Methods.

TIRF imaging

PC12 cells co-transfected with 1 μg pVenus-N1-NPY and RIM1 expression plasmids at the equal molar quantity (5.0 μg RIM1(11–399), 5.7 μg RIM1(400–1078), 5.0 μg RIM1(1079–1463), or 7.5 μg RIM1) and BADN (10 μg) using OptiFect (invitrogen) were plated onto poly-L-lysine-coated coverslips. PCR analysis reveals that the RIM plasmids are transfected at the equal level (Supplemetary Fig. 7b). The imaging was performed in modified Ringer's buffer. Fluorescence images of NPY-Venus were observed at the single vesicle level using an inverted microscope (IX71, Olympus). Incident light for total internal reflection illumination was introduced from the high numerical objective lens through a single mode optical fiber. Images were captured by a cooled CCD camera (EM-CCD, Hamamatsu Photonics). Area calculations and counting the number of fluorescent spots were performed using Metamorph softwares (Molecular Devices). The cells showing distribution of vesicles with < 10 μm^2 dark circle area, that can be placed in between vesicles, were selected as cells with uniformly distributed vesicles. 10 μm^2 was the maximal dark circle area in the images from BADN-transfected cells with uniform vesicle distribution. For details, see Supplementary Methods.

Immunostaining of cultured hippocampal neurons

Culture and transfection of mouse hippocampal neurons were essentially as described50. EGFP-tagged $Ca_v2.1$, myc-tagged RIM1, and FLAG-tagged β_{4b} were detected using a Zeiss LSM510META confocal microscope using a combination of antibodies: anti-FLAG M2 monoclonal, anti-myc polyclonal (Cell Signaling), Alexa488- and Alexa594-conjugated secondary antibodies (Invitrogen). See Supplemental Methods for further quantification procedures.

Current recordings

Whole-cell mode of the patch-clamp technique was performed at 22–25 °C. An external solution contained (in mM): 3 $BaCl_2$, 155 tetraethylammonium chloride (TEA-Cl), 10 HEPES, 10 glucose for BHK cells; 10 $BaCl_2$, 153 TEA-Cl, 10 HEPES, 10 glucose for PC12 cells (pH 7.4). The pipette solution contained (in mM): 95 CsOH, 95 Aspartate, 40 CsCl, 4 $MgCl_2$, 5 EGTA, 2 $ATPNa_2$, 5 HEPES, 8 creatine phosphate (pH 7.2). To characterize Ca^{2+}-dependent inactivation, external solutions contained (in mM): 5 $CaCl_2$ or $BaCl_2$, 153 TEA-Cl, 10 HEPES, 10 glucose (pH 7.4). The pipette solution contained (in mM): 135 Cs-$MeSO_3$, 5 CsCl, 0.5 EGTA, 5 $MgCl_2$, 4 $ATPNa_2$, 10 HEPES (pH 7.2). Single-channel currents were recorded using cell-attached patch mode. The bath solution contained (in mM): 150 KCl, 5 HEPES, 0.2 EGTA, 10 glucose (pH 7.4). The pipette solution contained (in mM): 110 $BaCl_2$ and 10 HEPES (pH 7.4). 750-ms voltage steps were given every 5 s from a V_h of −100 mV. Details of current recordings and analyses including voltage dependence of inactivation and activation and AP train are described in Supplementary Methods.

Suppression of the action of endogenous RIMs using siRNAs and BADN in PC12 cells

The sense siRNA sequences 5′-AAGAATGGACCACAAATGCTT-3′ and 5′-AAGGTGATTGGATGGTATAAA-3′ for rat RIM1, and 5′-AAGGCCCAGATACTCTTAGAT-3′ and 5′-AAGAACTATCCAACATGGTAA-3′ for rat RIM2 were used. Suppression of RNA expression was confirmed using RT-PCR analyses (Supplemetary Fig. 7a). The cells transfected with 8.0 μg pCI-neo-BADN or 8.0 μg pCI-neo-RIM1 were subjected to current recordings 72–96 h after transfection. For details, see Supplementary Methods.

Release assay and RNA analysis in PC12 cells

RNA expression of the α_1-subunits, β-subunits, RIM1, or RIM2 in PC12 cells was determined by RT-PCR (Supplemetary Fig. 7a,c; see Supplementary Table 9 for primers). ACh secretion experiments were performed as previously reported with slight modifications42. PC12 cells were plated in poly-D-lysine-coated 35-mm dishes (BD bioscience) with 5×10^5 cells per dish. Cells were co-transfected with 1 μg of pEFmChAT encoding mouse ChAT cDNA and RIM1 plasmids at equal molar quantity (3.4 μg of RIM1(11–399), 3.8 μg of RIM1(400–1078), 3.4 μg of RIM1(1079–1463), or 5.0 μg of RIM1) and BADN (10 μg) using Lipofectamine™ 2000 (invitrogen). Three days after transfection, ACh secretion experiments were performed. For details, see Supplementary Methods

Glutamate release assay using cerebellar neuron primary cultures

Cerebellar granular cells were plated on polyethylenimine-coated 35-mm diameter culture dishes (BD Falcon) at a density of $4.5–5.0 \times 10^6$ cells/dish. BADN or RIM1 cDNAs were introduced using Sindbis viruses in cerebellar neurons. 24 h after infection, high-K^+-evoked glutamate release were performed. For details, see Supplementary Methods.

Statistical analysis

All data accumulated under each condition from at least three independent experiments were expressed as means ± S.E.M. Student's t -test, Kolmogorov-Smirnov test, or ANOVA followed by Fisher's test was employed.

Ackowledgements:

We thanks A. Miyawaki for NPY-Venus, R. Y. Tsien for mCherry, S. Ozawa for pSinEGdsp vector, H. Hibino, H Atomi, and H. Okuno for helpful discussions, K. Yamazaki, K. Ueda, N. Yokoi and Y. Honjo for expert experiments, and K. Sugimoto and T. Morii for molecular modeling. This study was supported by research grants from the Ministry of Education, Culture, Sports, Science and Technology of Japan, the Japan Society for the Promotion of Science, and Human Frontier Science Program. K.P.C. is an Investigator of the Howard Hughes Medical Institute.

Footnotes:

Supplementary information is available on the Nature Neuroscience website.

Author contributions

S.K., M.W., T.M., and Y.U. acquisition, analysis and interpretation of data, and drafting of the manuscript; H.B., A.M.B., M.T., and K.P.C., analysis and interpretation of data, and drafting of the manuscript; E.M., Y.H., M.N., M.D.W., M.K., and M.I., acquisition, analysis and interpretation of data; Y.M., analysis and interpretation of data, and drafting and critical review of the manuscript.

Competing interests statement

The authors declare that they have no competing financial interests.

References:

- 1. Zhai RG , Bellen HJ The architecture of the active zone in the presynaptic nerve terminal. Physiology. 19: 262- 270 2004;
- 2. Atwood HL Gatekeeper at the synapse. Science. 312: 1008- 1009 2006;
- 3. Neher E Vesicle pools and Ca^{2+} microdomains: New tools for understanding their roles in neurotransmitter release. Neuron. 20: 389- 399 1998;
- 4. Wang Y , Okamoto M , Schmitz F , Hofmann K , Südhof TC Rim is a putative Rab3 effector in regulating synaptic-vesicle fusion. Nature. 388: 593- 598 1997;
- 5. Wang Y , Südhof TC Genomic definition of RIM proteins: evolutionary amplification of a family of synaptic regulatory proteins. Genomics. 81: 126- 137 2003;
- 6. Wang Y , Sugita S , Südhof TC The RIM/NIM family of neuronal C_2 domain proteins. J Biol Chem. 275: 20033- 20044 2000;
- 7. Betz A Functional interaction of the active zone proteins Munc13-1 and RIM1 in synaptic vesicle priming. Neuron. 30: 183- 196 2001;
- 8. Ohtsuka T CAST: a novel protein of the cytomatrix at the active zone of synapses that forms a tenary complex with RIM1 and Munc13-1. J Cell Biol. 158: 577- 590 2002;
- 9. Schoch S RIM1α forms a protein scaffold for regulating neurotransmitter release at the active zone. Nature. 415: 321- 326 2002;
- 10. Coppola T Direct interaction of the Rab3 effector RIM with Ca^{2+} channels, SNAP-25, and synaptotagmin. J Biol Chem. 276: 32756- 32762 2001;
- 11. Castillo PE , Schoch S , Schmitz F , Südhof TC , Malenka RC RIM1α is required for presynaptic long-term potentiation. Nature. 415: 327- 330 2002;
- 12. Calakos N , Schoch S , Südhof TC , Malenka RC Multiple roles for the active zone protein RIM1α in late stages of neurotransmitter release. Neuron. 42: 889- 896 2004;
- 13.. Tsien RW , Ellinor PT , Horne WA Molecular diversity of voltage-dependent Ca^{2+} channels. Trends Pharmacol Sci. 12: 349- 354 1991;
- 14.. Takahashi T , Momiyama A Different types of calcium channels mediate central synaptic transmission. Nature. 366: 156- 158 1993;
- 15. Wheeler DB , Randell A , Tsien RW Roles of N-type and Q-type Ca^{2+} channels in supporting hippocampal synaptic transmission. Science. 264: 107- 111 1994;
- 16. Catterall WA Structure and function of neuronal Ca^{2+} channels and their role in neurotransmitter release. Cell Calcium. 24: 307- 323 1998;
- 17.. Ertel EA Nomenclature of voltage-gated calcium channels. Neuron. 25: 533- 535 2000;
- 18. Sheng ZH , Rettig J , Takahashi M , Catterall WA Identification of a syntaxin-binding site of N-type calcium channels. Neuron. 13: 1303- 1313 1994;
- 19. Bezprozvanny I , Scheller RH , Tsien RW Functional impact of syntaxin on gating of N-type and Q-type calcium channels. Nature. 378: 623- 626 1995;
- 20. Zhong H , Yokoyama CT , Scheuer T , Catterall WA Reciprocal regulation of P/Q-type Ca^{2+} channels by SNAP-25, syntaxin and synaptotagmin. Nat Neurosci. 2: 939- 941 1999;
- 21. Spafford JD , Zamponi GW Functional interactions between presynaptic calcium channels and the neurotransmitter release machinery. Curr Opin Neurobiol. 13: 308- 314 2003;
- 22.. Maximov A , Südhof TC , Bezprozvanny I Association of neuronal calcium channels with modular adaptor proteins. J Biol Chem. 274: 24453- 24456 1999;
- 23.. Maximov A , Bezprozvany I Synaptic targeting of N-type calcium channels in hippocampal neurons. J Neurosci. 22: 6939- 6952 2002;
- 24. Nishimune H , Sanes JR , Carlson SS A synaptic laminin-calcium channel interaction organizes active zones in motor nerve terminals. Nature. 432: 580- 587 2004;
- 25. Kang MG A functional AMPA receptor-calcium channel complex in the postsynaptic membrane. Proc Natl Acad Sci USA. 103: 5561- 5566 2006;
- 26. Mori Y Primary structure and functional expression from complementary DNA of a brain calcium channel. Nature. 350: 398- 402 1991;
- 27. Bichet D The I–II loop of the Ca^{2+} channel α_1 subunit contains an endoplasmic reticulum retention signal antagonized by the β subunit. Neuron. 25: 177- 190 2000;
- 28. Varadi G , Lory P , Schultz D , Varadi M , Schwartz A Acceleration of activation and inactivation by the β subunit of the skeletal muscle calcium channel. Nature. 352: 159- 162 1991;
- 29. Béguin P Regulation of Ca^{2+} channel expression at the cell surface by the small G-protein kir/Gem. Nature. 411: 701- 706 2001;
- 30. Hibino H Direct interaction with a nuclear protein and regulation of gene silencing by a variant of the Ca^{2+}-channel β_4 subunit. Proc Natl Acad Sci USA. 100: 307- 312 2003;
- 31. Vendel AC Alternative splicing of the voltage-gated Ca^{2+} channel β_4 subunit creates a uniquely folded N-terminal protein binding domain with cell-specific expression in the cerebellar cortex. J Neurosci. 26: 2635- 2644 2006;
- 32. Burgess DL β subunit reshuffling modifies N- and P/Q-type Ca^{2+} channel subunit compositions in lethargic mouse brain. Mol Cell Neurosci. 13: 293- 311 1999;
- 33. Opatowsky Y , Chen CC , Campbell KP , Hirsch JA Structural analysis of the voltage-dependent calcium channel β subunit functional core and its complex with the α_1 interaction domain. Neuron. 42: 387- 399 2004;
- 34. Khanna R , Li Q , Sun L , Collins TJ , Stanley EF N type Ca^{2+} channels and RIM scaffold protein covary at the presynaptic transmitter release face but are components of independent protein complexes. Neuroscience. 140: 1201- 1208 2006;
- 35.. Plummer MR , Logothetis DE , Hess P Elementary properties and pharmacological sensitivities of calcium channels in mammalian peripheral neurons. Neuron. 2: 1453- 1463 1989;
- 36. Patil PG , Brody DL , Yue DT Preferential closed-state inactivation of neuronal calcium channels. Neuron. 20: 1027- 1038 1998;
- 37. De Waard M , Pragnell M , Campbell KP Ca^{2+} channel regulation by a conserved β subunit domain. Neuron. 13: 495- 503 1994;
- 38. DeMaria CD , Soong TW , Alseikhan BA , Alvania RS , Yue DT Calmodulin bifurcates the local Ca^{2+} signal that modulates P/Q-type Ca^{2+} channels. Nature. 411: 484- 489 2001;
- 39.. Stanley EF Syntaxin I modulation of presynaptic calcium channel inactivation revealed by botulinum toxin C1. Eur J Neurosci. 17: 1303- 1305 2003;
- 40. Dulubova I A Munc13/RIM/Rab3 tripartite complex: from priming to plasticity?. EMBO J. 24: 2839- 2850 2005;
- 41. Liu H Expression and subunit interaction of voltage-dependent Ca^{2+} channels in PC12 cells. J Neurosci. 16: 7557- 7565 1996;
- 42. Nishiki T Comparison of exocytotic mechanisms between acetylcholine- and catecholamine-containing vesicles in rat pheochromocytoma cells. Biochem Biophys Res Commun. 239: 57- 62 1997;
- 43. Zhang JF , Ellinor PT , Aldrich RW , Tsien RW Molecular determinants of voltage-dependent inactivation in calcium channels. Nature. 372: 97- 100 1994;
- 44. Stotz SC , Hamid J , Spaetgens RL , Jarvis SE , Zamponi GW Fast inactivation of voltage-dependent calcium channels. J Biol Chem. 275: 24575- 24582 2000;
- 45.. Geib S The interaction between the I–II loop and the III–IV loop of $Ca_v2.1$ contributes to voltage-dependent inactivation in a β-dependent manner. J Biol Chem. 277: 10003- 10013 2002;
- 46. Weimer RM UNC-13 and UNC-10/Rim localize synaptic vesicles to specific membrane domains. J Neurosci. 26: 8040- 8047 2006;
- 47.. Schoch S Redundant functions of RIM1α and RIM2α in Ca^{2+}-triggered neurotransmitter release. EMBO J. 25: 5852- 5863 2006;
- 48. Hibino H RIM binding proteins (RBPs) couple Rab3-interacting molecules (RIMs) to voltage-gated Ca^{2+} channels. Neuron. 34: 411- 423 2002;
- 49. Koushika SP A post-docking role for active zone protein Rim. Nat Neurosci. 4: 997- 1005 2001;
- 50. Nonaka M , Doi T , Fujiyoshi Y , Takemoto-Kimura S , Bito H Essential contribution of the ligand-binding βB/βC loop of PDZ1 and PDZ2 in the regulation of postsynaptic clustering, scaffolding, and localization of postsynaptic density-95. J Neurosci. 26: 763- 774 2006;

Figure 1

Direct interaction of RIM1 with the VDCC β_{4b}-subunit

(**a**) Domain structure of mouse RIM1. Arrows indicate molecules interacting with RIM1 at the Zn^{2+}-finger like domain (Zn^{2+}); PDZ domain (PDZ); first and second C_2 domains (C_2A and C_2B); proline-rich region (PXXP)4,6-10. The protein region encoded by clone #2-5 is also indicated. (**b**) Mapping of RIM1 binding sites on β_{4b} by the yeast two-hybrid assay. β-subunit constructs in bait vectors are tested with RIM1 in the prey vector. The interactions are scored by β-galactosidase activity and His^+ prototrophy. (**c**) Pulldown assay of β_{4b} with GST fusion RIM1 mutants. GST fusion proteins immobilized on glutathione-Sepharose beads are incubated with cell lysate obtained from myc-β_{4b} -transfected HEK293 cells. Bound proteins are analyzed by western blotting (WB) using anti-myc antibody. (**d**) in vitro association between the purified GST-RIM1 fusion constructs and recombinant β_4-subunit (47–475). GST-RIM1 proteins at various concentrations, incubated with β_4 (50 pM), are captured by glutathione-Sepharose beads. Captured β_4 proteins are examined by WB. The bottom panel shows the quantitative densitometric analysis of bands shown in the upper panel and in Supplementary Fig. 2. The saturation curves are subjected to the nonlinear least-squares curve-fitting method to evaluate the apparent dissociation constant (K_d). (**e**) Interaction of recombinant β_{4b} and RIM1 in HEK293 cells. The interaction is evaluated by immunoprecipitation (IP) with anti-FLAG antibody, followed by WB with anti-myc antibody. Top: physical association of myc-β_{4b} with FLAG-RIM1 in comparison to a positive control FLAG-$Ca_v2.1$(I–II linker). Bottom: physical association of FLAG-β_{4b} with myc-RIM1.

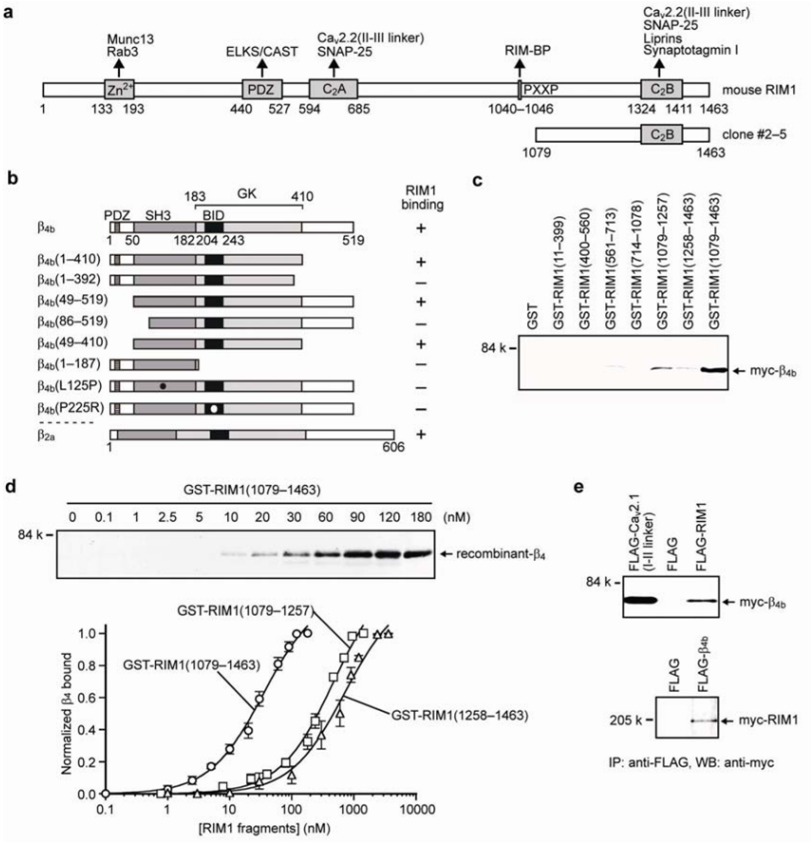

Figure 2

Association of RIM1 with native neuronal VDCC complexes

(**a**) Sucrose gradient fractionation of neuronal VDCC complexes from wild-type (WT) mouse brains and subsequent WB demonstrate cosedimentation of RIM1 with $Ca_v2.1$ and β_4. Syntaxin showed similar cosedimentation with RIM1. (**b**) Densitometry of $Ca_v2.1$, β_4, and RIM1 from western blots of sucrose gradient fractions. The normalized density of each protein is plotted as a function of the sucrose density fraction number. (**c**) Coimmunoprecipitation of RIM1 with the β_4-subunit. Immunoprecipitation (IP) using an anti-β_4 antibody and subsequent WB for RIM1 is performed on heparin purified samples. As a negative control, a preparation from lethargic mice is used. (**d**) Sucrose gradient fractionation of neuronal VDCC complexes from lethargic mouse brains. (**e**) Coimmunoprecipitation of $Ca_v2.1$ with RIM1. The immunocomplexes are disrupted by GST-BADN or GST-RIM1(1079–1463). IP using anti-RIM1 antibody and subsequent WB for $Ca_v2.1$ is performed.

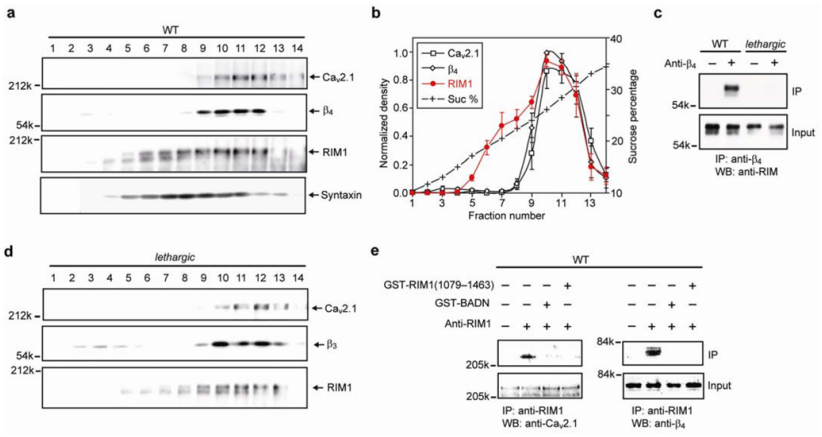

Figure 3

RIM1 clusters with the VDCC subunits near presynaptic termini in cultured hippocampal neurons

(**a**) $Ca_v2.1$ elicits plasma membrane (PM) colocalization of β_{4b} with RIM1. BADN disrupts colocalization. Left: confocal imaging of HEK293 cells expressing EGFP-β_{4b} and RIM1-DsRedmonomer with vector, $Ca_v2.1$, or $Ca_v2.1$ plus BADN. Scale bar: 5 μm. Nuclei are stained with Hoechst 33342. Right: subcellular location of EGFP-β_{4b} or RIM1-DsRedmonomer in 1 μm widths PM region and in the cytosolic area (CYT) (n = 5). *** P < 0.001 vs vector. ## P < 0.01 vs $Ca_v2.1$. (**b**) β_{4b} elicits PM colocalization of $Ca_v2.1$(I–II linker) and RIM1. BADN disrupts colocalization. Left: confocal imaging of HEK293 cells expressing CD8-$Ca_v2.1$(I–II linker)-EGFP and RIM1-DsRedmonomer with vector, β_{4b}, or β_{4b} and BADN. Right: subcellular location of CD8-$Ca_v2.1$(I–II linker)-EGFP or RIM1-DsRedmonomer (n = 5). *** P < 0.001 vs vector. ## P < 0.01 vs β_{4b}. (**c**) Immunolocalization of tagged-RIM1 and β_{4b} in cultured hippocampal neurons. Clustering of RIM1 and β_{4b} is undetected at 8 DIV, but present at a substantially later stage at 23 DIV. Scale bar: 10 μm. (**d**) Late clustering of EGFP-$Ca_v2.1$ (arrowheads) in hippocampal neurons. Synapsin I-positive puncta are already abundant at 8 DIV, while $Ca_v2.1$ distribution is still diffuse. Like RIM1 and β_{4b}, $Ca_v2.1$ clusters much later on. (**e, f**) Accumulation of EGFP-$Ca_v2.1$ (arrowheads) in presynaptic varicosities is achieved between 9 and 22 DIV. This maturation process is impaired by RIM1(1079–1463) or BADN, suggesting that the local VDCC concentration at AZs is influenced by RIM1-β-subunit interaction during a postsynaptogenic maturation period.

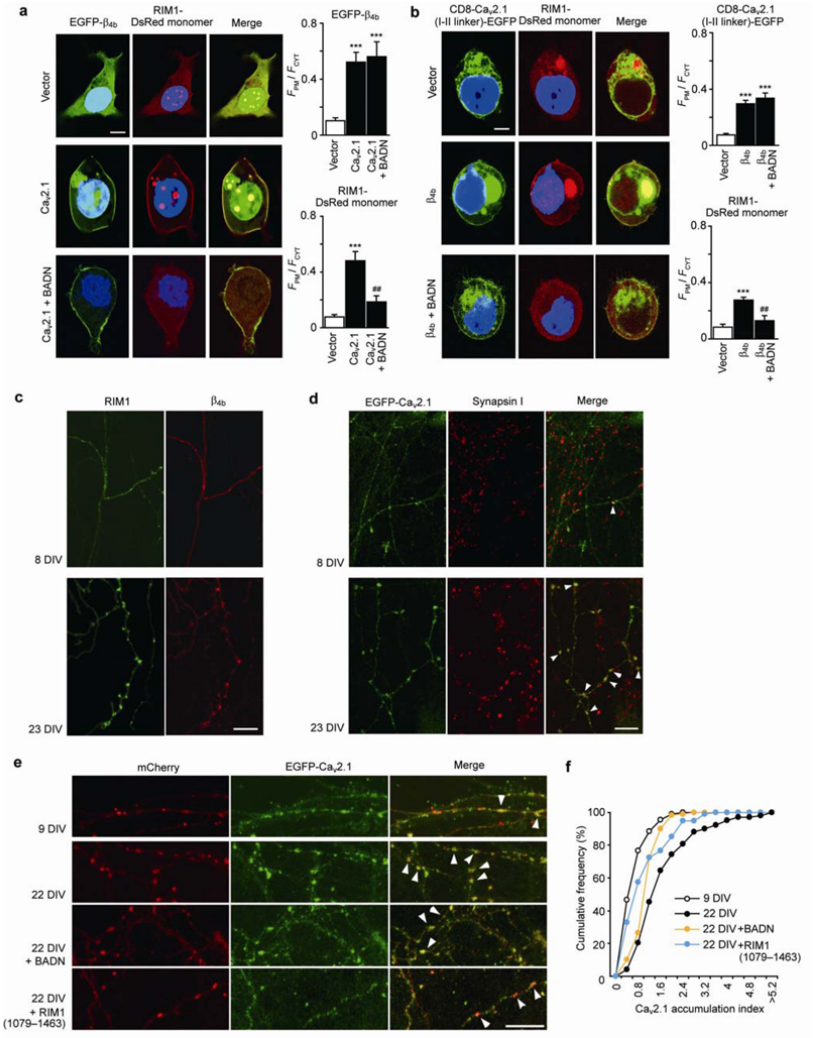

Figure 4

Effects of RIM1 on the inactivation properties of recombinant neuronal VDCCs

(**a**)Inactivation of P/Q-type $Ca_v2.1$ currents in BHK cells. The peak amplitudes before and after coexpression of RIM1 constructs are normalized for Ba^{2+} currents elicited by 2-s pulses to 0 mV from a holding potential (V_h) of −100 mV. (**b**) Inactivation of N-type $Ca_v2.2$, R-type $Ca_v2.3$, or L-type $Ca_v1.2$ currents (with β_{4b}). The V_h is −100 mV ($Ca_v2.2$, $Ca_v1.2$) or −110 mV ($Ca_v2.3$). (**c**) Left: inactivation curves for $Ca_v2.1$ (with β_{1a}). Right: inactivation curves for $Ca_v2.1$ in BHK cells expressing α_2/δ and different β-subunits. See Supplementary Table 2 and 3 for statistical significance of the differences. (**d**) Inactivation curves for $Ca_v2.2$, $Ca_v2.3$ (left), or $Ca_v1.2$ (right) (with β_{4b}). See Supplementary Table 1 for statistical significance of the differences. (**e**) RIM1 prolongs the time between first channel opening and last closing within a single-channel trace of $Ca_v2.1$ (with β_{4b}). Seven consecutive unitary traces are shown. The mean values for the time of each trace are 184.2 ± 33.3 ms (n = 117 traces) for vector and 502.8 ± 33.3 ms, (n = 101) for RIM1. The time for traces without opening is counted as 0 ms. (**f**) Left: $Ca_v2.1$ currents (with β_{1a}) induced by 100 Hz AP trains for 1 s. Right: percentage of currents in response to the last stimulus compared to the peak current (n = 6 for vector and n = 4 for RIM1). *** $P < 0.001$.

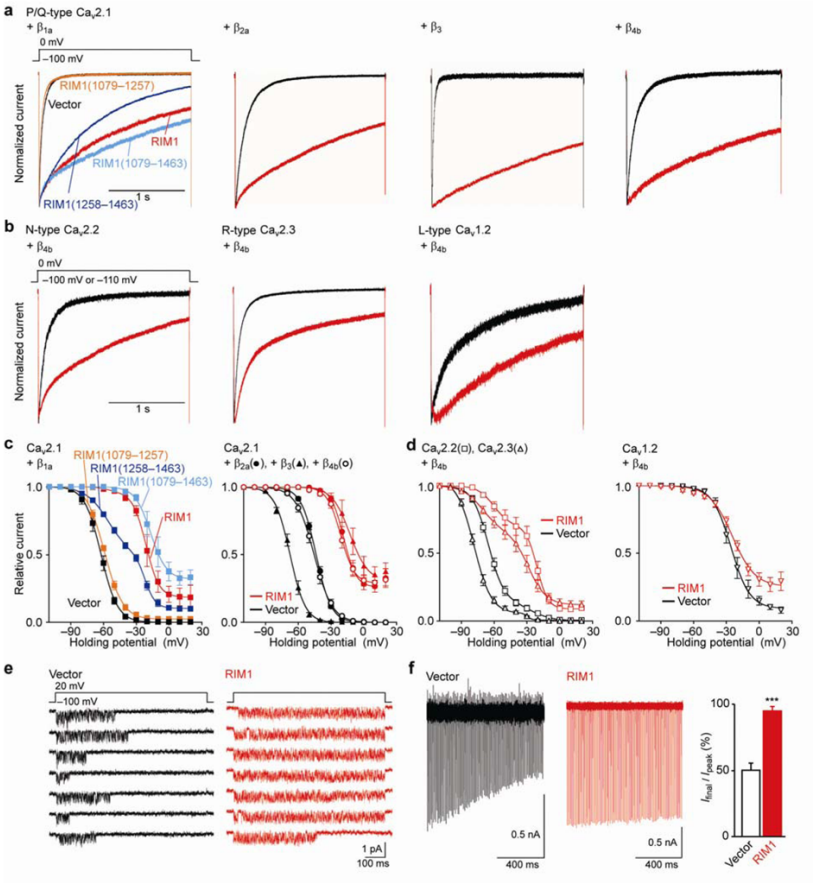

Figure 5

Physiological relevance of effects of RIM1 on inactivation properties of VDCCs

(**a**) Effects of RIM1 on inactivation time courses of $Ca_v2.1$ Ba2+ and Ca^{2+} currents (with β_1) in HEK293 cells. The peak amplitudes before and after RIM1 coexpression are normalized for Ba^{2+} and Ca^{2+} currents elicited by 2-s pulses to 0 and 10 mV, respectively, from a V_h of −80 mV. (**b**) Inactivation curves for $Ca_v2.1$ Ba2+ and Ca^{2+} currents (with β_1) in HEK293 cells. See Supplementary Table 6 for statistical significance of the differences. (**c**) Effects of RIM1 and BADN on the inactivation properties of native VDCCs in PC12 cells (7–9 culture passage). Left: normalized current traces. Middle: inactivation curves induced by 2-s holding potential displacement. See Supplementary Table 7 for statistical significance of the differences. Right: comparison of current densities at 10 mV (n = 18, 15, and 9 cells for vector, RIM1, and BADN, respectively). (**d**) Acceleration of inactivation by coapplication of siRNAs specific for RIM1 and RIM2 (siRIM1 and siRIM2) in VDCC currents recorded from PC12 cells (2–3 culture passages). Left: normalized current traces. Middle: inactivation curves. See Supplementary Table 7 for statistical significance of the differences. Right: comparison of current densities at 10 mV (n = 6 and 8 cells, for siControl and siRIM1 and siRIM2, respectively).

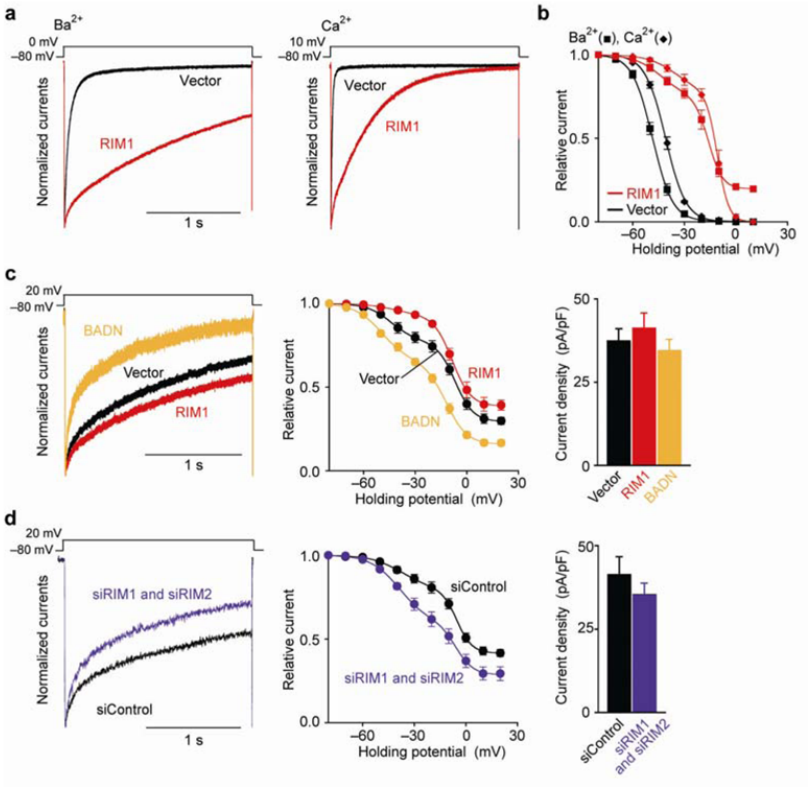

Figure 6

Effects of RIM1 on the activation properties of VDCCs

(**a**) Effects of RIM1 on activation curves of Ca_v currents (with β_{4b}) elicited in BHK cells. Tail currents elicited by repolarization to −60 mV after 5-ms test pulse from −50 to 50 mV are used to determine activation curves. See Supplementary Table 1 for statistical significance of the differences. (**b**) Left: effects on activation speed of $Ca_v2.1$ channels containing various β-subunits. Time constants are obtained by fitting the activation phase of currents elicited by 5-ms test pulse to 20 mV with a single exponential function. Right: effects of RIM1 on activation speed of Ca_v currents at 20 mV in various VDCC types. * $P < 0.05$ and *** $P < 0.001$. (**c**) Effects of RIM1 proteins on P/Q-type $Ca_v2.1$. Left: representative traces for Ba^{2+} currents (with β_{4b}) upon application of test pluses from −40 mV to 50 mV with 10-mV increments. Right: current density-voltage (I–V) relationships of $Ca_v2.1$. The V_h is −100 mV. See Supplementary Table 2 for statistical significance of the differences. (**d**) I–V relationships of $Ca_v2.2$ (left) and $Ca_v2.3$ or $Ca_v1.2$ (right) (with β_{4b}). The V_h is −100 mV ($Ca_v2.2$, $Ca_v1.2$) or −110 mV ($Ca_v2.3$). See Supplementary Table 1 for statistical significance of the differences.

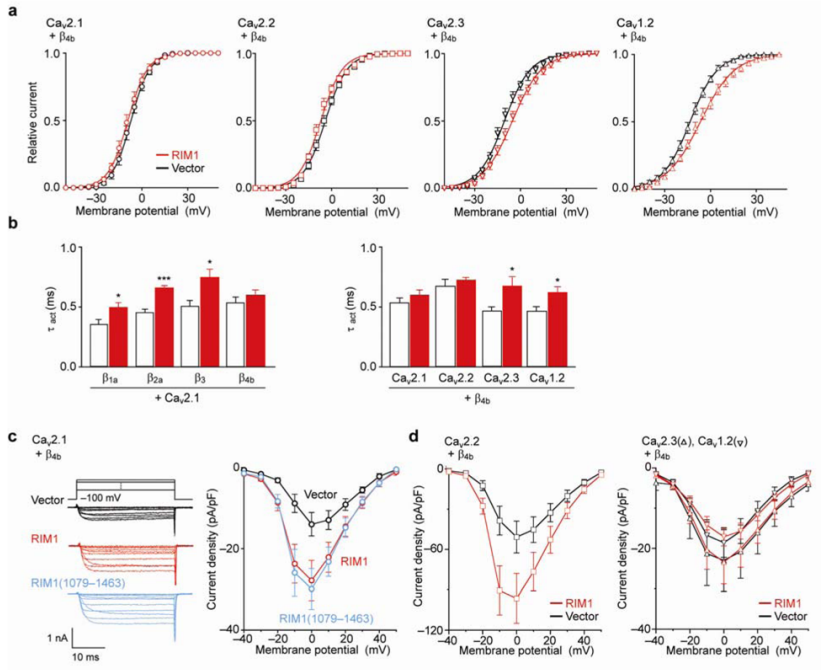

Figure 7

RIM1 and β-subunits associate to anchor neurotransmitter vesicles to VDCCs at the plasma membrane

(**a**) NPY-containing secretory vesicles are colocalized with RIM1 and VAMP, that is not colocalized with caveolin-1 in PC12 cells. NPY-Venus and RIM1-DsRedmonomer, VAMP-Venus and RIM1-DsRedmonomer, NPY-Venus and VAMP-DsRedmonomer, or caveolin-1-EGFP and VAMP-DsRedmonomer are coexpressed in PC12 cells, and live images of the cells are obtained by confocal microscopy. Scale bar: 10 μm. (**b,c**) Effects of RIM1 constructs and BADN on the density of docked vesicles. In **b**, typical TIRF images of plasma membrane-docked vesicles containing NPY-Venus. Left: BADN-co-transfected PC12 cell. Middle: vector-co-transfected PC12 cell. Right: RIM1-co-transfected PC12 cell. Scale bar: 10 μm. In **c**, the vesicle density is determined by counting the vesicles in each image (n = 20 cells in each). * $P < 0.05$, *** $P < 0.001$ vs vector. $^{\#\#\#}$ $P < 0.001$ vs RIM1.

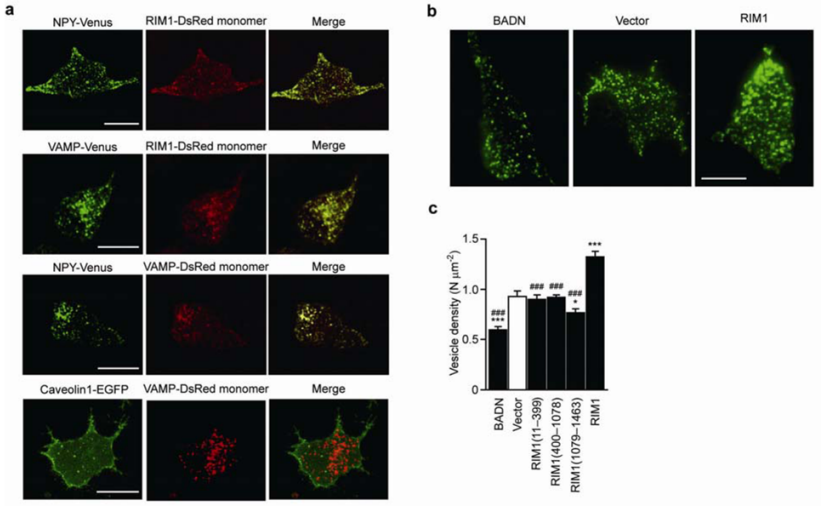

Figure 8

The RIM1-β association enhances neurotransmitter release in PC12 cells and cultured cerebellar neurons

(**a**) Effects of RIM1 constructs and BADN on depolarization-dependent release of ACh from ChAT-co-transfected PC12 cells. Three days after transfection, PC12 cells were incubated for 30 s with the low-K^+ solution (5.9 mM K^+) at 37 °C. The release of ACh during this period was considered as basal release. To measure ACh release, the cells were then incubated for 30 s with a high-K^+ solution (51.1 mM K^+). The amount of secreted ACh is determined as a percentage of the cellular content for each dish. *** $P < 0.001$ vs vector. $^{\#\#}$ $P < 0.01$, $^{\#\#\#}$ $P < 0.001$ vs RIM1. (**b**) Effects of RIM1 and BADN on depolarization-dependent release of glutamate from cultured cerebellar neurons. 24 h after the introduction of cDNAs, cerebellar neurons (9–11 DIV) were incubated for 1 min with the low-K^+ solution (5.9 mM K^+) at 37 °C. The release of glutamate during this period was considered as basal release. To measure glutamate release, the cells were then incubated for 1 min with a high-K^+ solution (51.1 mM K^+). * $P < 0.05$.